"PAPER FOR YOUNG SCIENTIST AWARD"

Unsteady Electro-osmotic analysis of Multiphase immiscible nanofluids (Casson-Jeffrey) under the magnetic field in an asymmetric channel

Sangeetha J.

Department of Mathematics, National Institute of Technology, Tiruchirappalli, Tamil Nadu, India-620015.
E-mail: sangeethajagan009@gmail.com

ABSTRACT

The investigation has been carried out on the convective multiphase time-dependent flow of Casson-Jeffrey and Newtonian nanofluids in an asymmetric channel under the effect of electroosmotic force along with the magnetic field. The mathematical model has been formulated using the governing system of continuity, momentum and temperature equations. The present model was analysed analytically using periodic function to obtain the velocity profiles, temperature distribution and entropy generation. Furthermore, a parametric study was performed to analyse the traits of different nanoparticle volume fractions and their transport characteristics over the (mineral oil and ethylene glycol) base fluids with (gold, silver, copper, palladium, titanium oxide and Iron) nanoparticles examined and the results are demonstrated in graphical aspects. It was found that the Gold and Palladium particles were performed highly compared to the rest of the nanoparticles.

Keywords: Hybrid fluid, Nanofluids, Palladium, Gold, Time-dependent.

1. INTRODUCTION

In recent developments, the performance of nanofluids is utilized in diverse features of fluid systems which are incorporated as heat transportation in the thermal engineering systems. The significant performance of nanofluids was very efficient compared to the regular fluids in the form of heat carriers in the thermal engineering fields to utilized in applications such as power plants, cooling systems, thermal management in the building, vehicle air-conditioning systems in transportation, heat pipes in-space propulsions, solar collector systems and geo-thermic systems. To enhance the thermal conductivity, Choi[1] introduced the nanofluid for the substitution of conventional fluids by incorporating the nano-sized particles which are probably metallic in nature into the base fluids like oil, water and other fluids. From their work, the significance of nanofluids becomes tremendous in various fields including biomedical engineering. Followed by them, many scientific researchers simulated the model in theoretical and experimental form to understand the performance of nanofluids in various circumstances. Esfe et al. [2] experimentally proposed a model based on the thermal conductivity of Zinc-oxide and Ethylene Glycol and computed using the ANN method. Based on the flow of blood in the stenosed artery, the suspension of drug particles in the stream was analysed by Ponalagusamy [3]. Numerical simulation has been carried out on the multilayer flow of immiscible viscous fluid in the rectangular duct by Umavathi and

Basavarajappa [4] for various types of nanofluids. Marwa et al. [5] interpreted their view on the application of palladium, a noble metal nanoparticle in various aspects.

Since then, many scientists have studied and discovered the single-phase flow of nanoparticles. Apart from single-phase fluid, multiphase fluids have a wide range of applications in the form of immiscible behaviour on the combination of non-Newtonian fluid and Newtonian fluid. Based on this idea, Micheal Bentwich [6] analysed the flow of two-phase immiscible fluids in the axial tube based on the oil pipeline data. Ponalagusamy and Sangeetha [7] discussed the electrodynamic effects of immiscible traits in Thixotropic-Newtonian fluids. Apart from dealing with immiscible features, the authors of this study focused on the nature of mixed non-Newtonian models of Jeffrey and Casson fluids to establish the theoretical results in different aspects. Such combined fluids are called Hybrid fluids. In our research, the formulations have been taken on the behaviour of Jeffrey and Casson fluids. Hayat et al. [8] analytically solved the mixed convection stagnation point of Casson fluid. The oscillating flow of Casson fluid with slip condition was formulated analytically by Imran et al. [9]. Sreenadh et al. [10] investigated the immiscible flow of Jeffrey fluid in an elastic tube. Sangeetha and Ponalagusamy [11] formulated the unsteady peristaltic behaviour of Jeffery fluid in an elastic tube under the electromagnetic hydrodynamic effect. Abbas and Wasfi [12] investigated the Casson-Micropolar nanofluid on the Stretching Riga Sheet. Casson-Williamson flow in the microchannel under the hall effects was performed numerically by Gireesha and Anitha [13].

So far, the discussion over the electric and magnetic field on the hybrid nanofluids was least discussed. Coulomb law formulates the behaviour of the electric field, meanwhile, the magnetic field obeys the Lorentz law. These two forces act on the fluids to make an effective motion. So, the influence of electromagnetic force retains its control over the other forces. Harshad et al. [14] discussed the interfacial influence of electroosmotic transport on the electrically conducting and non-conducting fluids. Ponalagusamy and Sangeetha [15] performed the analytical approach on the Electroosmotic effect on Casson-Newtonian fluids under a magnetic field. MHD behaviour on nanofluids was interpreted by Salahuddin et al [16] providing the performance of different kinds of nanofluids under a magnetic field. Sangeetha et al. [17,18] formulated the effectiveness of the external electric field in the immiscible non-newtonian and Newtonian forms.

Whenever dealing with thermal analysis, the interesting phenomenon was the minimisation of entropy generation which benefits from reducing the irreversibility by constructing an innovative thermal management system. Decreasing the entropy generation will improve the efficiency of the energy generated in the closed system. Based on this concept, Xie and Jian [19] intervened in the characteristics entropy generation of two fluid electroosmotic flows. On the combination of single and hybrid nanofluids projected in the thermal systems, the minimization of entropy generation was reviewed by Gabriela and Angela [20]. Numerical investigation was analysed based on the entropy systems in the rotating microchannel by Eegunjobi and Makinde [21]. Chandan et al. [22] deal with the entropy generation of two-phase blood flow through a stenosed artery along with variable viscosity.

For all the aforementioned experimental and theoretical studies this research article is constructed based on the following discussion. The model description and the solution of the problem were studied in analytical form. The graphical aspects were presented with the validation results along with the explanation. Finally ended with the consolidation results in the conclusion section.

2. PROBLEM FORMULATION

Model description

The features involved in the model to analyze the convective laminar incompressible flow subjected to electromagnetic effect are depicted in Fig.1, which consisting two immiscible fluids in an asymmetric channel. In Fig 1, the lower region ($-h_1 \leq y \leq 0$) is assumed as a hybrid fluid which possesses the properties of electrically non-conducting nanofluid. Meanwhile, the upper region ($0 \leq y \leq h_2$) is categorized as electrically conducting nanofluid. The conduit wall is isothermal and maintains different temperatures and the no-slip velocity acts at the wall. Since the fluid layers are maintained the interconnectedness which results in the continuity of tangential velocity/heat transfer and stress/heat flux produces the balance over it.

Mathematical construction

1) **Electric potential:**

Based on the electrostatic theory, the symmetric distribution of ions in the electrolyte solution was expressed in the Poisson equation (1D from) as net charge density and potential distribution,

$$\frac{d^2\psi^*}{dr^*} = -\frac{\rho_e^*}{\epsilon_p} \quad \textbf{(1)}$$

The charge density for symmetric electrolytes is described by Boltzmann distribution as

$$\rho_e^* = -2z_1 e n_1 \, sinh\left(\frac{ez_1}{k_b T_b}\psi^*\right) \quad \textbf{(2)}$$

After substituting and Debye-Hückel approximation we get,

$$\frac{d^2\psi^*}{dr^{*2}} = -\frac{2z_1 e n_1}{\epsilon_p} \, sinh\left(\frac{ez_1}{k_b T_b}\psi^*\right) \cong -\frac{2z_1^2 e^2 n_1}{\epsilon_p k_b T_b}\psi^* = k^{*2}\psi^* \quad \textbf{(3)}$$

Where, $k^{*2} = -\frac{2z_1^2 e^2 n_1}{\epsilon_p k_b T_b}$; along with the boundary conditions, $y^* = 0; \psi^* = \psi_I^*; y^* = h_2; \psi^* = \psi_w^*$. After incorporating following dimensionless quantities $y = \frac{y^*}{h}; \psi_I = \frac{\psi_I}{\psi}; \psi_w = \frac{\psi_w}{\psi}$, we obtain

$$\frac{d^2\psi}{dr^2} = k^2\psi; \text{ at } y = 0; \ \psi = \psi_I; y = h_2; \psi = \psi_w. \quad \textbf{(4)}$$

Solving along with the corresponding boundary condition, we get

$$\psi = \psi_I \cosh(ky) + \left(\frac{\psi_w - \psi_I \cosh(kh_2)}{\sinh(kh_2)}\right)\sinh(ky) \quad \textbf{(5)}$$

Analytical solution for Temperature, Velocity and Energy generation:

Based on the aforementioned model descriptions, the field of momentum and temperature equations in both regions are displayed as follows,

Region I ($-h_1^* \le y^* \le 0$):

$$\rho_1^*\left(\frac{\partial w_1^*}{\partial t^*}\right) = -\frac{\partial p^*}{\partial z^*} + \left[\frac{\mu_1^*}{1+\lambda} + \frac{\mu_1^*}{\beta}\right]\frac{\partial^2 w_1^*}{\partial y^{2^*}}(E_0 - B_0^* w_1^*)\sigma_1 B_0^* + (\rho\alpha_T)^* g^*(T_1^* - T_w^*) \quad \textbf{(6)}$$

$$(\rho C_P)_1^*\left(\frac{\partial T_1^*}{\partial t^*}\right) = K_1^*\left(\frac{\partial^2 T_1^*}{\partial y^{2^*}}\right) - \frac{\partial q_1^*}{\partial y^*} + Q_s^* \quad \textbf{(7)}$$

Region II ($0 \le y^* \le h_2^*$):

$$\rho_2^*\left(\frac{\partial w_2^*}{\partial t^*}\right) = -\frac{\partial p^*}{\partial z^*} + \mu_2^*\frac{\partial^2 w_c^*}{\partial y^{2^*}}(E_0 - B_0^* w_2^*)\sigma_2 B_0^* + \rho_e^* E_z^* e^{i\omega_e t} + (\rho\alpha_T)^* g^*(T_2^* - T_w^*) \quad \textbf{(8)}$$

$$(\rho C_P)_2^*\left(\frac{\partial T_2^*}{\partial t^*}\right) = K_2^*\left(\frac{\partial^2 T_2^*}{\partial y^{2^*}}\right) - \frac{\partial q_2^*}{\partial y^*} + Q_s^* \quad \textbf{(9)}$$

We have adopted the following non-dimensional quantities.

$$u_i = \frac{u_i^*}{U_{HS}}; p = \frac{H^*}{U_{HS}\mu_{b_2}^*}p^*; z = \frac{z^*}{H^*}; h_i = \frac{h_i^*}{H^*}; t = t^*\omega; y = \frac{y^*}{H^*}; \ \theta_i = \frac{T_i^* - T_0^*}{T_w^* - T_0^*}; \mu_r = \frac{\mu_{b_1}^*}{\mu_{b_2}^*}; \quad \textbf{(10)}$$

$$Pe = \frac{(\rho C_p)_{b_2}\omega H^{*2}}{K_{b_2}}; N^2 = \frac{4(\alpha_T)_{b_2}^2 H^{*2}}{K_{b_2}}; Q = \frac{Q_s H^{*2}}{(T_w^* - T_0^*)K_{b_2}}; \ \alpha^* = \frac{\rho_{b_2}\omega H^{*2}}{\mu_{b_2}^*}; K_r = \frac{K_{b_1}}{K_{b_2}}; E = \frac{E_0}{B_0 U_{HS}};$$

$$Gr = \frac{(\rho\alpha_T)_{b_2} g^*(T_w^* - T_0^*)H^*}{U_{HS}\mu_{b_2}^*}; \ M^2 = \frac{\sigma_{b_2} B_0^2 H^{*2}}{\mu_{b_2}}; S = \frac{E_0 H^*}{U_{HS}}\sqrt{\frac{\sigma_{b_2}}{\mu_{b_2}}}; \Omega_0 = \frac{T_w^* - T_0^*}{T_0^*}; Br = \frac{\mu_{b_2}^* U_{HS}^2}{K_{b_2}(T_w^* - T_0^*)}.$$

After substituting we get,
Region I:

$$\alpha_1^2 \frac{\partial w_1}{\partial t} = P + \mu_1 \left(\frac{1}{1+\lambda} + \frac{1}{\beta}\right) \frac{\partial^2 w_1}{\partial y^2} + S_1 M_1 - M_1^2 w_1 + Gr_1 \theta_1 \quad \textbf{(11)}$$

$$Pe_1 \frac{\partial \theta_1}{\partial t} = \frac{\partial^2 \theta_1}{\partial y^2} - N_1^2 \theta_1 + Q_1 \quad \textbf{(12)}$$

Region II:

$$\alpha_2^2 \frac{\partial w_2}{\partial t} = P + \mu_2 \frac{\partial^2 w_2}{\partial y^2} + S_2 M_2 - M_2^2 w_2 + Gr_2 \theta_2 + \frac{d^2 \psi}{dy^2} e^{i\omega_e t} \quad \textbf{(13)}$$

$$Pe_2 \frac{\partial \theta_2}{\partial t} = \frac{\partial^2 \theta_2}{\partial y^2} - N_2^2 \theta_2 + Q_2 \quad \textbf{(14)}$$

With dimensionless boundary conditions,

$$at\ y = 0; w_1 = w_2;\ \tau_1 = \tau_2 + \tau_{elec};\ \theta_1 = \theta_2;$$

$$at\ y = h_2; w_2 = 0; \theta_2 = 0; at\ y = h_1; w_1 = 0; \theta_1 = 0; \quad \textbf{(15)}$$

Here, we adopted the following method to solve the equations,

$$w_i(y,t) = w_{0i}(y) e^{i\omega t}, \theta_i(y,t) = \theta_{0i}(y) e^{i\omega t} \quad \textbf{(16)}$$

Region I:

$$w_1 = C_1 \cosh(z_3 y) + C_2 \sinh(z_3 y) + \frac{\left(P + \frac{Gr_1 Q_1}{z_1^2}\right)}{\mu_1 \left(\frac{1}{1+\lambda} + \frac{1}{\beta}\right) z_4^2} - \frac{Gr_1 A_1}{\mu_1 \left(\frac{1}{1+\lambda} + \frac{1}{\beta}\right)} V_1 - \frac{Gr_1 B_1}{\mu_1 \left(\frac{1}{1+\lambda} + \frac{1}{\beta}\right)} V_2 \quad \textbf{(17)}$$

$$\theta_1 = A_1 \cosh(z_1 y) + B_1 \sinh(z_1 y) + \frac{Q_1}{z_1^2} \quad \textbf{(18)}$$

Region II:

$$w_2 = C_3 \cosh(z_4 y) + C_4 \sinh(z_4 y) + \frac{\left(P + \frac{Gr_2 Q_2}{z_2^2}\right)}{\mu_2 z_4^2} - \frac{Gr_2 A_2}{\mu_2} V_3 - \frac{Gr_2 B_2}{\mu_2} V_4 - \frac{\kappa^2}{\mu_2} \left\{ \begin{matrix} \zeta_I V_5 + \\ \left[\frac{\zeta_w - \zeta_I \cosh(kh_2)}{\sinh(kh_2)}\right] V_6 \end{matrix} \right\} \quad \textbf{(19)}$$

$$\theta_2 = A_2 \cosh(z_2 y) + B_2 \sinh(z_2 y) + \frac{Q_2}{z_2^2} \quad \textbf{(20)}$$

Where, $z_1^2 = N_1^2 + i\omega Pe_1; z_2^2 = N_2^2 + i\omega Pe_2; z_3^2 = \frac{i\omega \alpha_1^2 + M_1^2}{\mu_1 \left(\frac{1}{1+\lambda} + \frac{1}{\beta}\right)}; z_4^2 = \frac{i\omega \alpha_2^2 + M_2^2}{\mu_2};$

The minimization of entropy generation,

$$S_{gen_1}^* = \frac{K_1^*}{T_0^{*2}} \left(\frac{\partial T_1^*}{\partial r^*}\right)^2 + \frac{\tau_{rz_1}^*}{T_0^*} \left(\frac{\partial w_1^*}{\partial r^*}\right) + \frac{\sigma^*}{T_0^*} (B_0^* w_1^* - E_0^*)^2; -h_1^* \le y^* \le 0. \quad \textbf{(21)}$$

$$S_{gen_2}^* = \frac{K_2^*}{T_0^{*2}} \left(\frac{\partial T_2^*}{\partial r^*}\right)^2 + \frac{\tau_{rz_2}^*}{T_0^*} \left(\frac{\partial w_2^*}{\partial r^*}\right) + \frac{\sigma^*}{T_0^*} (B_0^* w_2^* - E_0^*)^2;\ 0 \le y^* \le h_2^*. \quad \textbf{(22)}$$

The non-dimensional form as

$$S_1 = \left(\frac{d\theta_1}{dy}\right)^2 + \frac{Br_1}{\Omega_0}\left(\frac{1}{1+\lambda}+\frac{1}{\beta}\right)\left(\frac{dw_1}{dy}\right)^2 + \frac{M_1^2 Br_1}{\Omega_0}(w_1 - E_0)^2 \quad \textbf{(23)}$$

$$S_2 = \left(\frac{d\theta_2}{dy}\right)^2 + \frac{Br_2}{\Omega_0}\left(\frac{dw_2}{dy}\right)^2 + \frac{M_2^2 Br_2}{\Omega_0}(w_2 - E_0)^2 \quad \textbf{(24)}$$

Where, the constant we displayed in appendices.

4. FIGURES AND TABLES

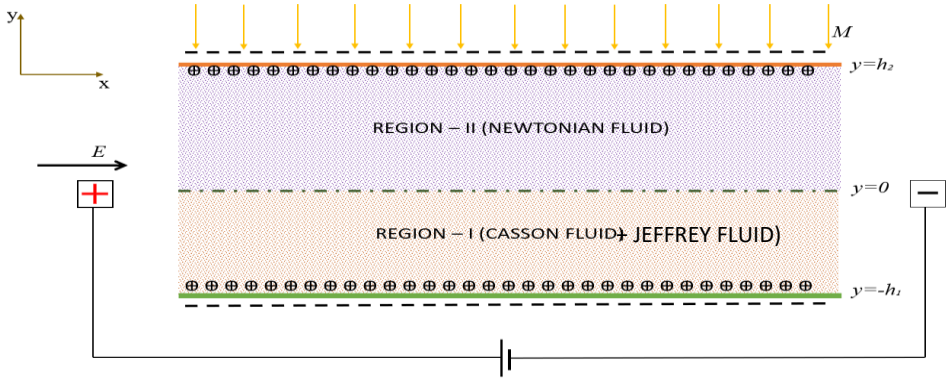

Figure 1. Under the impact of electric and magnetic forces, a pictorial representation of the suggested model is shown.

Table 1: The sphericity of the nanoparticles

	Sphere	Cylinder	Bricks	Platelets	Blade	Tetrahedron	Hexahedron	Octahedron
Shape factor	3	4.9	3.7	5.7	8.9	4.06	3.72	1.18

Table 2: Thermophysical properties of the fluids

Density	$\rho_i = (1-\phi_i)\rho_{b_i} + \phi_i \rho_{s_i}$	Thermal conductivity	$K_i = K_{b_i}\left(\frac{K_{s_i} + (n_2-1)K_{b_i} + (n_2-1)\phi_i(K_{s_i}-K_{b_i})}{K_{s_i} + (n_2-1)K_{b_i} - \phi_i(K_{s_i}-K_{b_i})}\right)$
Thermal Expansion Coefficient	$(\rho\alpha_T)_i = (1-\phi_i)(\rho\alpha_T)_{b_i} + \phi_i(\rho\alpha_T)_{s_i}$	Heat Capacitance	$(\rho C_p)_i = \phi_i(\rho C_p)_{s_i} + (1-\phi_i)(\rho C_p)_{b_i}$
Viscosity	$\mu_i = \frac{\mu_{b_i}}{(1-\phi_i)^{2.5}}$	Electrical Conductivity	$\sigma_i = \sigma_{b_i}\left(\frac{\sigma_{s_i} + 2\sigma_{b_i} - 2\phi_i(\sigma_{b_i}-\sigma_{s_i})}{\sigma_{s_i} + 2\sigma_{b_i} + \phi_i(\sigma_{b_i}-\sigma_{s_i})}\right)$

Table 3: Thermophysical properties of base and particles at room temperature.

	Density (Kg/m^3)	Thermal Conductivity (W/mK)	Thermal expansion (K^{-1}) $x10^{-5}$	Viscosity ($kg\ m^{-1}s^{-1}$) $X10^{-3}$	Heat Capacitance (J/Kg K)	Electrical Conductivity (S/m)
Mineral Oil	920	0.121	64	0.0145	1670	$1x10^{-11}$
Ethylene Glycol	1114	0.252	57	0.0157	2420	$5.5x10^{-6}$
Gold	19320	314	1.67		129.1	$4.5x10^{7}$
Silver	10500	429	1.89		233	$6.2x10^{7}$
Copper	8933	401	1.67		390	$5.9x10^{7}$
Iron	7870	80	58		470	$1x10^{7}$
Palladium	12023	72	117.7		240	$1x10^{7}$
Titanium oxide	4250	8.9538	84		686.2	$2.38x10^{6}$

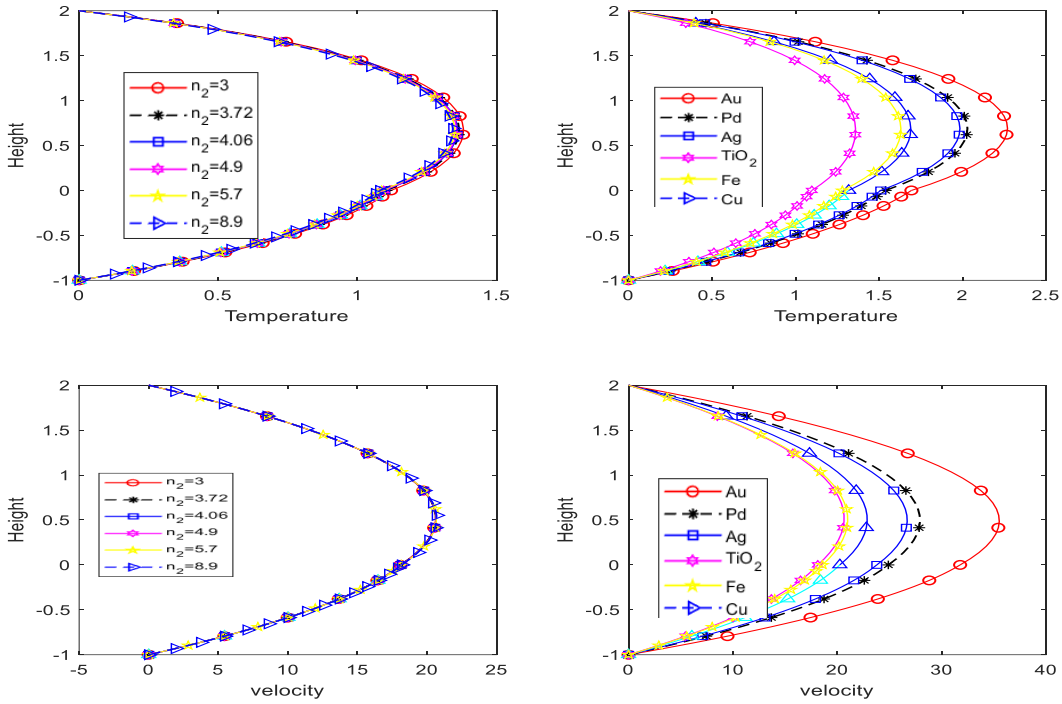

Fig 2: Temperature and velocity profiles for different values of nano particles and sphericity

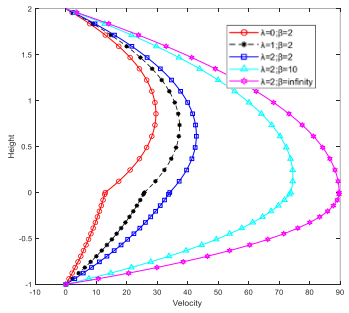

Fig 3: velocity profiles for different values of Casson (β) and Jeffery (λ) parameters

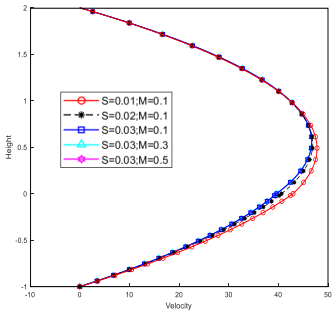

Fig 4: velocity profiles for different values of Magnetic parameter (S) and Hartmann number (M).

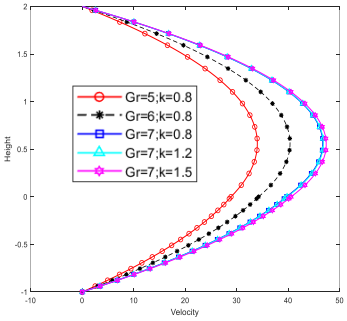

Fig 5: velocity profiles for different values of Grashof number (Gr) and electroosmotic parameter (k).

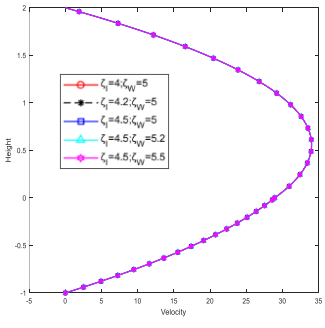

Fig 6: velocity profiles for different values of zeta potential at wall (ζ_w) and Interface (ζ_I).

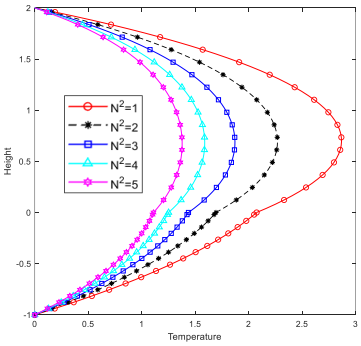

Fig 7: Temperature profiles for different values of Heat radiation parameters.

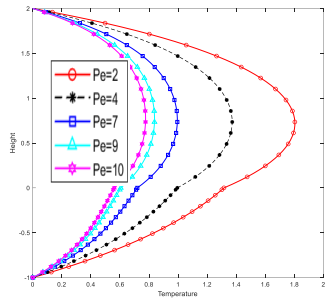

Fig 8: Temperature profiles for different values of Peclet number.

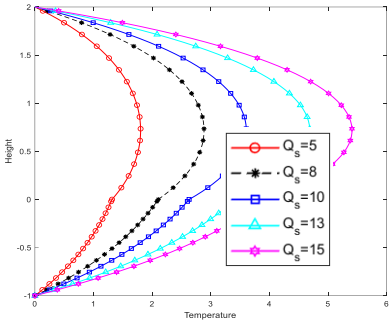

Fig 9: Temperature profiles for different values of source/sink parameters.

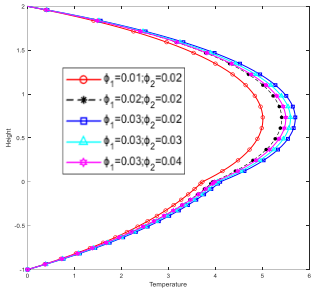

Fig 10: Temperature profiles for different values of nano volume fraction.

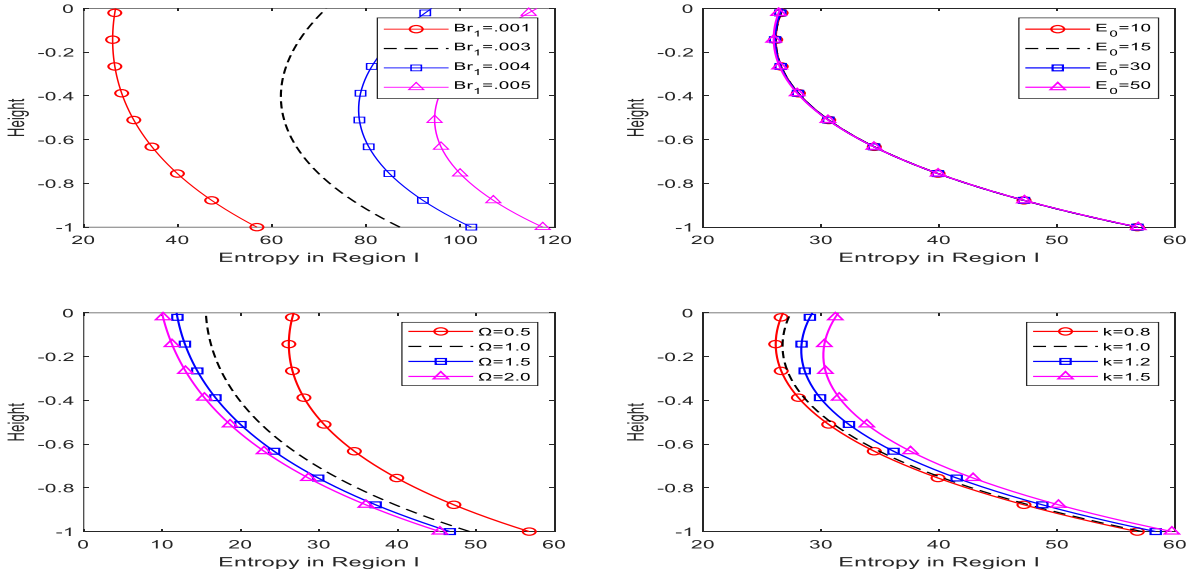

Fig 11: Entropy generation of specified parameters in the region I.

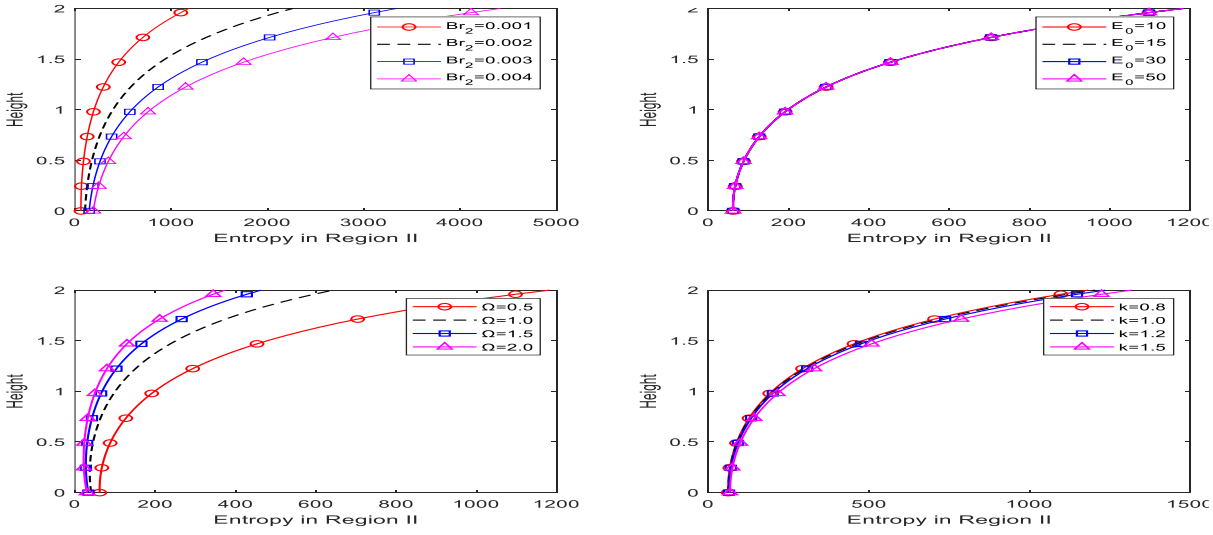

Fig 12: Entropy generation of specified parameters in the region II.

5. RESULT AND DISCUSSIONS

Velocity and temperature validation analysis

In Figure 2, we performed the validation of the choice of base fluids and nanoparticles. In our study we considered the fluid present in the lower region i.e. Region I was treated as a hybrid fluid as possessing the traits of ethylene glycol meanwhile, the fluid present in the upper region i.e. region II was assumed to be mineral oil. In addition to that, we have assumed the various nanoparticles such as Gold, Silver, Palladium, Titanium Oxide, Iron and Copper along with the sphericity which is shown in Table 1. Figure 2 (a & c), analysed the temperature and velocity along with sphericity. It is shown that increasing the sphericity enhanced the velocity and decreased the temperature. Simultaneously, In Figure 2 (b & d), the various thermal physical properties of nanoparticles displayed in Table 3 were taken into account. In these figures, we analysed that the temperature distribution was lower and the velocity was higher in the following order Gold, Palladium, Silver, Titanium Oxide, Iron and Copper. In such a case we have taken that the effective nanoparticles such as Gold and Palladium. The Gold nanoparticles were subjected to the ethylene glycol base fluid meanwhile Palladium nanoparticles were used for mineral oil base fluid.

Analyzation of velocity profiles

The subsequent influence of the axial velocities through the asymmetric channel under the impact of various parameters like Casson parameter (β), Jeffrey Parameter (λ), Magnetic parameter, Hartmann number, Grashof numbers, electro-osmotic parameter and electric potential in Figures 3-6. In Figure 3, we discussed the influence of hybrid nanofluids such as Casson and Jeffrey fluid. In this figure, we demonstrated the velocity profiles are increased for the increasing values of Jeffrey and Casson Parameters. These parameters influence the fluid present in Region II due to the interfacial continuity effects. In Figure 4, the magnetic parameters exposed by maxwell electromagnetic induction and the Hartmann number produced by external magnetic field were shown. In this figure, we observed that in both cases, the velocities of the fluids in both regions decreased for the increasing values of the Magnetic parameter and Hartmann number. The velocity profiles for the variation of Grashof numbers and electroosmotic effect were analysed in Figure 5. In this diagram, we observed the enhancement were occurred for the increasing values of the Grashof number and electroosmotic parameter. The zeta potential of the external electric field at

the interface and wall region was analysed in Figure 6. It is noticed that the velocity of the fluids was increased for the increased values of zeta potential due to the continuity of interfacial at shear stress in the formation of the Electric double-layer effect.

Analyzation of temperature profiles

The intervention of the temperature distribution over various parameters was portrayed in Figures 7-10 using the values displayed in Table 2-4 for the corresponding thermophysical properties. In Figure 7, the heat radiation parameters made an effective route for reducing the temperature distribution. For the increasing values of Peclet numbers, the temperature profiles were decreased as displayed in Figure 8. The variation of temperature distribution over the given region to the provided heat source/sink parameters for the two layers is displayed in Figure 9. From this figure, we can observe that the enhancement of heat source and sink upsurge the temperature in both regions. In Figure 10, it is shown the impact of the size of the nanoparticles over the thermal conduction. The dissipation of the heat has occurred clearly for the increment of size (ϕ_1 & ϕ_2) of the particles. This results in a reduction in the temperature of the fluids. Moreover, this substantiates that the addition of nanoparticles behaves as a coolant.

Analyzation of entropy generation

The variation of entropy generation in both regions concerning specified parameters for Brinckmann numbers, electric field, Temperature parameter and electroosmotic parameters was studied in Figures 11(a-d) and 12(a-d). In Figure 11(a), the enhancement of entropy in the lower region was shown for the increased values of Brickman numbers even for the small increment. Similarly, the same result was obtained for the increased values of the electric field possessed by the influence of maxwell electromagnetic force displayed in Figure 11(b). In Figure 11(c), the impact of the Temperature parameter was declined whereas the electroosmotic parameter was upsurged in entropy generation. The same traits were observed in the upper region (region-II) with similar attributes.

CONCLUSION

The investigation was carried out on the influence of nanofluids on combined non-newtonian (electrically non-conducting) and Newtonian (conducting) fluids in an asymmetric channel under the effect of electroosmotic technique along with magnetic field in the form of velocity profiles, temperature distribution and entropy generation. The outcomes of the present study are summarized as follows:

- The influence of the electric field, Magnetic field, Grashof number, Peclet number, nano-volume fraction and nano-particle sizes was observed and found that the velocities increased for the electric field, nano-volume fraction and nano-particle sizes increased whereas increasing the magnetic field tended to reduce the velocity of fluids.
- In temperature distribution, we noticed the temperature decreased for the larger size and shapes of the nanoparticles.
- The effect of an external electric field possesses a dual nature in the interfacial region and the wall region.
- The entropy generation produced in both regions was analysed under the influence of Brinckmann number, Electric field, Temperature parameter and electroosmotic parameter.
- The entropy generation in both regions increased for enhanced values of Brinckmann number, Electric field and electroosmotic parameter whereas declined for higher values of Temperature parameter.
- Jeffery-Newtonian, Casson-Newtonian and Newtonian-Newtonian models can be deduced from the present work.
- The effectiveness of Gold and palladium nanofluids was much more efficient than the rest of the nanoparticles which was studied in this research.

APPENDIX

$$B_2 = \frac{\left[\frac{Q_1}{z_1^2}(\cosh(z_1h_1)-1)-\frac{Q_2}{z_2^2}\cosh(z_1h_1)\right]\cosh(z_2h_2)+\frac{Q_2}{z_2^2}\cosh(z_1h_1)}{(z_2/K_rz_1)\cosh(z_2h_2)\sinh(z_1h_1)-\cosh(z_1h_1)\sinh(z_2h_2)}; A_2 = -\frac{\left[\frac{Q_2}{z_2^2}+B_2\sinh(z_2h_2)\right]}{\cosh(z_2h_2)};$$

$$B_1 = \frac{z_2}{K_rz_1}B_2; A_1 = A_2 + \frac{Q_2}{z_2^2} - \frac{Q_1}{z_1^2}; C_4 = \frac{MC\cosh(z_4h_2)+MB\cosh(z_3h_1)}{\gamma}; \mu_r = \frac{\mu_1}{\mu_2}; \Omega = \left(\frac{1}{1+\lambda}+\frac{1}{\beta}\right);$$

$$C_1 = \frac{z_3}{\mu_r\Omega}\left(\frac{C_4}{z_4} - \omega_2 - \omega_1\right); C_2 = C_3 + \omega_4 - \omega_3; C_3 = -\frac{MB+C_4\sinh(z_4h_2)}{\cosh(z_4h_2)};$$

$$\omega_3 = \frac{\left(P+\frac{Gr_1Q_1}{z_1^2}\right)}{\mu_1\Omega z_4^2} + \frac{Gr_1A_1}{\mu_1\Omega}S_2 + \frac{Gr_1B_1}{\mu_1\Omega}S_4;$$

$$\omega_4 = \frac{\left(P+\frac{Gr_2Q_2}{z_2^2}\right)}{\mu_2z_4^2} + \frac{Gr_2A_2}{\mu_2}S_6 + \frac{Gr_2B_2}{\mu_2}S_8 - \frac{\kappa^2}{\mu_2}\left\{\zeta_lS_{10} + \left[\frac{\zeta_w-\zeta_l\cosh(kh_2)}{\sinh(kh_2)}\right]S_{12}\right\};$$

$$\omega_1 = \mu_r\left[\frac{Gr_1A_1s_1-Gr_2B_1s_3}{2z_3\mu_1}\right]; \Omega_2 = \frac{Gr_2(A_2s_5+B_2s_7)+\kappa^2\zeta_ls_9}{2\mu_2z_4} + \left[\frac{\xi_w-\zeta_l\cosh(kh_2)}{\sinh(kh_2)}\right]\left(\frac{\kappa^2s_{11}}{2\mu_2z_4} - \frac{1}{\kappa}\right);$$

$$\gamma = \frac{z_3}{\mu_r\Omega z_4}\cosh(z_4h_2)\sinh(z_3h_1) - \cosh(z_3h_1)\sinh(z_4h_2);$$

$$MA = \frac{\left(P+\frac{Gr_1Q_1}{z_1^2}\right)}{\mu_1\Omega z_4^2} + \frac{Gr_1A_1}{\mu_1\Omega}(S_1\sinh(z_3h_1) + S_2\cosh(z_3h_1)) - \frac{Gr_1B_1}{\mu_1\Omega}(S_3\sinh(z_3h_1) - S_4\cosh(z_3h_1)).$$

$$MB = \frac{\left(P+\frac{Gr_2Q_2}{z_2^2}\right)}{\mu_2z_4^2} - \frac{Gr_2A_2}{\mu_2}(S_5\sinh(z_4h_2) - S_6\cosh(z_4h_2)) - \frac{Gr_2B_2}{\mu_2}(S_7\sinh(z_4h_2) - S_8\cosh(z_4h_2)) - \frac{\kappa^2}{\mu_2}\left\{\zeta_l(S_9\sinh(z_4h_2) - S_{10}\cosh(z_4h_2)) - \left[\frac{\zeta_w-\zeta_l\cosh(kh_2)}{\sinh(kh_2)}\right](S_{11}\sinh(z_4h_2) - S_{12}\cosh(z_4h_2))\right\}.$$

$$MC = \frac{z_3}{\mu_r\Omega}(\omega_2+\omega_1)\sinh(z_3h_1) - MA - (\omega_4-\omega_3)\cosh(z_3h_1).$$

$$S_1 = \left[\frac{\sinh(z_3+z_1)h_1}{z_3+z_1} + \frac{\sinh(z_3-z_1)h_1}{z_3-z_1}\right]; S_2 = \left[\frac{1}{z_3+z_1} + \frac{1}{z_3-z_1} - \frac{\cosh(z_3+z_1)h_1}{z_3+z_1} - \frac{\cosh(z_3-z_1)h_1}{z_3-z_1}\right];$$

$S_3 = \left[\frac{1}{z_1+z_3} + \frac{1}{z_1-z_3} - \frac{\cosh(z_1+z_3)h_1}{z_1+z_3} - \frac{\cosh(z_1-z_3)h_1}{z_1-z_3}\right]; S_4 = \left[\frac{\sinh(z_3-z_1)h_1}{z_3-z_1} - \frac{\sinh(z_3+z_1)h_1}{z_3+z_1}\right];$
$S_5 = \left[\frac{\sinh(z_2+z_4)h_2}{z_2+z_4} + \frac{\sinh(z_2-z_4)h_2}{z_2-z_4}\right]; S_6 = \left[\frac{\cosh(z_2+z_4)h_2}{z_2+z_4} + \frac{\cosh(z_4-z_2)h_2}{z_4-z_2} - \frac{1}{z_2+z_4} - \frac{1}{z_4-z_2}\right];$
$S_7 = \left[\frac{\cosh(z_2+z_4)h_2}{z_2+z_4} + \frac{\cosh(z_2-z_4)h_2}{z_2-z_4} - \frac{1}{z_2+z_4} - \frac{1}{z_2-z_4}\right]; S_8 = \left[\frac{\sinh(z_2+z_4)h_2}{z_2+z_4} - \frac{\sinh(z_2-z_4)h_2}{z_2-z_4}\right];$
$S_9 = \left[\frac{\sinh(z_4+\kappa)h_2}{z_4+\kappa} + \frac{\sinh(z_4-\kappa)h_2}{z_4-\kappa}\right]; S_{10} = \left[\frac{\cosh(z_4+\kappa)h_2}{z_4+\kappa} + \frac{\cosh(z_4-\kappa)h_2}{z_4-\kappa} - \frac{1}{z_4+\kappa} - \frac{1}{z_4-\kappa}\right];$
$S_{11} = \left[\frac{\cosh(z_4+\kappa)h_2}{z_4+\kappa} - \frac{\cosh(z_4-\kappa)h_2}{z_4-\kappa} - \frac{1}{z_4+\kappa} + \frac{1}{z_4-\kappa}\right]; S_{12} = \left[\frac{\sinh(z_4+\kappa)h_2}{z_4+\kappa} - \frac{\sinh(z_4-\kappa)h_2}{z_4-\kappa}\right];$
$V_1 = -\left[\frac{\sinh(z_3y)S_1 - \cosh(z_3y)S_2}{2}\right]; V_2 = \frac{\sinh(z_3y)S_3 - \cosh(z_3y)S_4}{2}; V_3 = \frac{\sinh(z_4y)S_5 - \cosh(z_4y)S_6}{2};$
$V_4 = \frac{\sinh(z_4y)S_7 - \cosh(z_4y)S_8}{2}; V_5 = \frac{\sinh(z_4y)S_9 - \cosh(z_4y)S_{10}}{2}; V_6 = \frac{\sinh(z_4y)S_{11} - \cosh(z_4y)S_{12}}{2};$

ACKNOWLEDGMENTS

The author was grateful for the sponsoring the fellowship provided by the MHRD through the NITT.

REFERENCES

1. Stephen U. S. Choi, Jeffrey A. Eastman, "Enhancing Thermal Conductivity of fluids with Nanoparticles", ASME International Mechanical Engineering Congress & Exposition 1995.
2. Mohammad Hemmat Esfe, Seyfolah Saedodin, Ali Naderi, Ali Alirezaie, Arash Karimipour, Somchai Wongwises, Marjan Goodarzi, Mahidzal bin Dahari, "Modelling of thermal conductivity of ZnO-EG using experimental data and ANN methods", International Communications in Heat and Mass Transfer 63 (2015) 35-40.
3. R. Ponalagusamy, "Particulate suspension Jeffrey fluid flow in a stenosed artery with a particle-free plasma layer near wall", Korea-Australia Rheology Journal, 28(3) 2016, 217-227.
4. Jawali C. Umavathi, Mahanthesh Basavarajappa, "Study of Multilayer flow of two immiscible nanofluids in a duct with viscous dissipation", physics of fluids 35 (2023) Article ID: 092018
5. Marwa Alaqarbeh, Syed Farooq Adil, Tamara Ghrear, Mujeeb Khan, Mohammed Bouachrine, Abdulrahman Al-Warthan, "Recent Progress in the Application of Palladium Nanoparticles: A Review", Catalysts, 13 (2023) 1343.
6. Micheal Bentwich, "Two-phase viscous axial flow in a pipe" Journal of Basic Engineering, 86, pp. 669-672, 1964.
7. R. Ponalagusamy, J. Sangeetha, "A study of electro-hydrodynamic flow of two immiscible fluids in a circular tube", 66th Congress of the Indian Society of Theoretical and Applied Mechanics (ISTAM) (An International Conference), 2021.
8. Hayat T, Shehzad SA, Alsaedi A, et al. Mixed convection stagnation point flow of Casson fluid with convective boundary condition. Chin Phys Lett 2012; 29: 114704
9. Imran MA, Sarwar S and Imran M. Effects of slip on free convection flow of Casson fluid over an oscillating vertical plate. Boundary Value Probl 2016; 30: 1–11.
10. Sreenadh Sreedharamalle, Sumalatha Baina, Srinivas A. N. S., "Flow of two immiscible non-Newtonian fluids in an elastic tube", World Journal of Engineering, 20(6) 2023 pp. 1174-1188.
11. J. Sangeetha, R. Ponalagusamy, "Unsteady Peristaltic Flow Of Two Immiscible Fluids In An Elastic Tube Under The Effect Of Electromagnetic Force Through The Porous Media", 68th Congress of the Indian Society of Theoretical and Applied Mechanics (ISTAM) (An International Conference), 2023.
12. Nadeem Abbas, Wasfi Shatanawi, "Heat and Mass Transfer of Micropolar-Casson Nanofluid over Vertical variable Stretching Riga Sheet", Energies, 15, 2022, 4945-2-20.
13. B. J. Gireesha, L. Anitha, "Repercussion of Hall effect and nonlinear radiation on Couette-Poiseuille flow of Casson-Williamson fluid through upright microchannel", Applied Mathematics and Mechanics, 43(12), 2022, 1951-1964.
14. Harshad Gaikwad, Dipankar Narayan Basu, Pranab Kumar Mondal, "Electroosmotic transport of immiscible binary system with a layer of non-conducting fluid under interfacial slip: The role applied pressure gradient", Electrophoresis, 00, 2016, 1-12.
15. Ramasamy Ponalagusamy, Jaganmohan Sangeetha, "Electroosmotic effect on two immiscible (conducting-non-conducting) fluids flowing in the porous channel under magnetic field", Proc IMech Part E: J Process Mechanical Engineering, 237(5) 2023 pp.2029-2044.
16. T. Salahuddin, Muhammad Habib Ullah Khan, Mair Khan, Basem Al Alwan, Abdelfattah Amari, "An analysis on the flow behavior of MHD nanofluid with heat generation", Fuel, 311 2022 122548.
17. J. Sangeetha, R. Ponalagusamy, R. Tamil Selvi, "Electroosmotic peristaltic flow of thixotropic-Newtonian fluids in a circular tube: Effect of variable viscosity co-efficient of core fluid" Chinese Journal of Physics 92 (2024) 470-493
18. Sangeetha J, Ponalagusamy R, "Electrokinetic Effect on 'Flow of Two-Phase Fluid in a Circular Tube", Sigma Journal of Engineering and Natural Sciences, Yildiz Technical University Press, Istanbul, Turkey, 2024. (In press)
19. Zhiyong Xie, Yongjun Jian, "Entropy generation of magnetohydrodynamic electroosmotic flow in two-layer systems with a layer of non-conducting viscoelastic fluid", International Journal of Heat and Mass Transfer, 127 (2018) 600-615.
20. Gabriela Huminic, Angel Huminic, "Entropy generation of nanofluid and hybrid nanofluid flow in thermal systems: A review", Journal of Molecular Liquids, 302 (2020) 112533.
21. Adetayo Samuel EEGUNJOBI, Oluwole Daniel MAKINDE, "Thermodynamics Analysis of an MHD Casson Fluid Flow Through a Rotating Permeable Channel with Slip and Hall Effects", Engineering Transactions, 68(3) 2020, 239-252.
22. Chandan Kumawat, B.K. Sharma, Qasem M. Al-Mdallal, Mohammad Rahimi-Gorji, "Entropy generation for MHD two phase blood flow through a curved permeable artery having variable viscosity with heat and mass transfer", International Communications in Heat and Mass Transfer 133 (2022) 105954.